

# Identification of Nonlinear Feedback Mechanisms Operating in Closed Loop using Inertial Sensors<sup>★</sup>

Fredrik Olsson<sup>\*</sup> Kjartan Halvorsen<sup>\*,\*\*\*</sup> Dave Zachariah<sup>\*</sup>  
Per Mattsson<sup>\*\*</sup>

<sup>\*</sup> Department of Information Technology, Uppsala University, Sweden  
(e-mails: [fredrik.olsson@it.uu.se](mailto:fredrik.olsson@it.uu.se), [kjartan.halvorsen@it.uu.se](mailto:kjartan.halvorsen@it.uu.se),  
[dave.zachariah@it.uu.se](mailto:dave.zachariah@it.uu.se)).

<sup>\*\*</sup> Department of Electronics, Mathematics and Natural Sciences,  
University of Gävle, Sweden (e-mail: [per.mattsson@hig.se](mailto:per.mattsson@hig.se))

<sup>\*\*\*</sup> Department of Mechatronics, Tecnológico de Monterrey, Mexico

**Abstract:** In this paper we study the problem of identifying linear and nonlinear feedback mechanisms, or controllers, operating in closed loop. A recently developed identification method for nonlinear systems, the LAVA method, is used for this purpose. Identification data is obtained from inertial sensors, that provide information about the movement of the system, in the form of linear acceleration and angular velocity measurements. This information is different from the information that is available to the controller to be identified, which makes use of unknown internal sensors instead. We provide two examples, a simulated neuromuscular controller in standing human balance, and a lead-filter controlling a physical position servo using a DC motor. Both linear and nonlinear controllers are used in the examples. We show that the LAVA method is able to identify sparse, parsimonious models of the controllers.

© 2018, IFAC (International Federation of Automatic Control) Hosting by Elsevier Ltd. All rights reserved.

*Keywords:* Closed-loop identification, Nonlinear control, Inertial sensors

## 1. INTRODUCTION

## 2. MODELING AND METHODS

Systems that operate in closed loop are controlled via feedback, and are typically designed such that the output of the system follows some reference signal. Often, the feedback controllers are designed based on a mathematical model of the system, which, for instance, can be obtained using system identification methods. However, there exists systems in nature that operate in closed loop and whose feedback controllers are unknown to us. For instance, feedback is ubiquitous in biological systems. The human balance system is one example, where the controller corresponds to the central nervous system (CNS), which senses the posture of the body and activates our muscles, such that we may stand upright against the forces of gravity instead of falling.

In this paper, we investigate the properties of the LAVA method, see Mattsson et al. (2018), for the case of identifying linear and nonlinear controllers operating in closed loop. The LAVA method was developed specifically for identification of nonlinear systems. Here, this method is used to estimate both linear and nonlinear controllers in two different cases, a simulated standing human balance scenario and a real-world controller in a position servo.

### 2.1 Identification of a controller operating in closed loop

We refer to a *plant* as some physical object which we may interact with through some input signal  $u$ . Interactions with the plant will affect its state and can be observed in the output  $y$ . System identification is most commonly used to construct mathematical models of plants that operate in open loop. In this work however, we are instead interested in plants that operate in closed loop, see Fig. 1, where  $u$  is chosen as the output of a controller. The controller can typically be seen as having two inputs, a reference signal  $r$  and (measurements of) the outputs  $y$  of the system to be controlled. The objective of the controller is then to choose  $u$  in order to bring the observed  $y$  as close to the reference signal  $r$  as possible. Some systems, for example biological systems, exist naturally as closed loop systems, where both the controller and the plant may be unknown.

In order for a controller, that operates in closed loop, to be identifiable, it is not sufficient that the plant output  $y$  provides sufficient excitation to the controller. As shown by Ljung (1999), an external excitation signal is also necessary to obtain data which facilitates identifiability. Therefore, we introduce an external disturbance signal  $d$ , as an additional input to the plant.

The data that is used to construct a model of the controller will be denoted by  $\mathcal{D}$ , and referred to as the identification data. The identification data consist of discrete-time mea-

<sup>★</sup> This work was supported by the project *Mobile assessment of human balance* (Contract number: 2015-05054), funded by the Swedish Research Council.

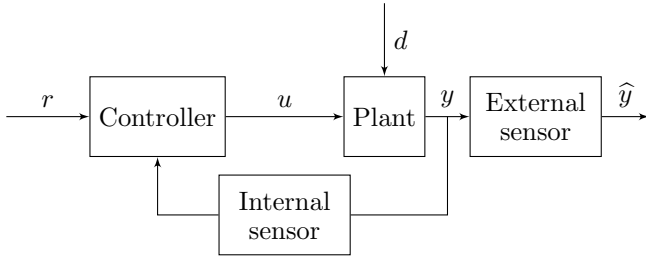


Fig. 1. A system operating in closed loop, with feedback provided by a controller.

measurements  $\hat{u}$  and  $\hat{y}$  of  $u$  and  $y$ , respectively

$$\mathcal{D} = \left\{ \left( \hat{u}(t), \hat{y}(t) \right) \right\}, \quad t = 1, \dots, N, \quad (1)$$

where  $t$  is the sample index and the data set consists of  $N$  measurements. We make use of information from external sensors to find the estimate  $\hat{y}$  of  $y$ . Note that the information we obtain about  $y$  may be different from the information that the controller receives, since the signal  $y$  is sensed in different ways (see Fig. 1). There may be unknown internal sensors that provides the controller with its own internal estimate of  $y$ , this is especially true in the case of biological systems. For example, our senses communicate information to the brain, which is used to control our actions, and generally we can not assume that any external sensor will provide the exact same information as the biological sensory systems, to our identification data. Therefore, it's important to keep in mind that the models we construct will be based on the information we have available, which is generally not the same information that the controller has available.

## 2.2 Inertial sensors

We make use of inertial sensors to collect the data used for identification. Inertial sensors consists of accelerometers, that measure linear acceleration, and gyroscopes, that measure angular velocity. These sensors are light-weight and have low power consumption, which makes them suitable for identification of systems where the output can be observed through movement. We will primarily use inertial sensors to obtain observations of the orientation and angular velocity in the experiments explained in Section 3 and Section 4. Sensor fusion of the accelerometer and gyroscope, and possibly a magnetometer that measures the local magnetic field, makes it possible to estimate the orientation of the sensor. Here, orientation estimates were obtained using an extended Kalman filter with orientation deviation states, see Kok (2016).

## 2.3 Method for nonlinear system identification

We begin by considering a linear dynamical predictor model of the controller output

$$u(t) = \Theta \varphi(t) + \varepsilon(t), \quad (2)$$

where  $\varphi(t)$  is the ARX regressor

$$\varphi(t) = [u^\top(t-1) \dots u^\top(t-n_a) \quad y^\top(t) \dots y^\top(t-n_b+1) \quad 1]^\top, \quad (3)$$

and  $n_a$  and  $n_b$  are non-negative integers, which decide the order of the linear predictor model. The matrix  $\Theta$  contains

the model parameters and  $\varepsilon(t)$  is the prediction error. This nominal linear predictor may describe the controller well around an operating point. However, as the controller deviates from this operating point, the errors  $\varepsilon(t)$  may become large due to model errors, and are typically poorly approximated by a white noise process as assumed in ARX-models.

In the LAVA-model, the nominal predictor (2) is extended by considering a data-driven model of the prediction errors:

$$\varepsilon(t)|\mathcal{D} \sim \mathcal{N}(Z\gamma(t), \Sigma) \quad (4)$$

where  $\gamma(t)$  is any given vector-valued function of past inputs and outputs,  $Z$  is a matrix of unknown parameters,  $\Sigma$  is an unknown covariance matrix. This error model can capture correlated data-dependent nominal prediction errors.

When the error model has been identified, the nominal predictor model (2) can be refined to

$$\hat{u}(t) = \hat{\Theta} \varphi(t) + \hat{Z} \gamma(t), \quad (5)$$

where the first term tries to capture linear structures in the data and the second term is an overparameterized error model that tries to capture deviations from the nominal linear predictor.

In this paper we let  $\gamma(t)$  be the Laplace basis expansion described in Solin and Särkkä (2014), due to its good approximation properties. In order to be able to describe general nonlinearities, we use quite long basis expansions, so that the number of elements in  $\gamma(t)$ , and thus  $Z$ , is large. That is, we overparameterize the model.

The identification method used is the latent variable (LAVA) approach in Mattsson et al. (2018), which is based on the maximum likelihood principle, and uses a majorization-minimization approach to tackle the resulting non-convex optimization problem. This results in a method that regularizes the overparameterized model learning towards the linear predictor class in a data-adaptive manner and seeks a sparse parameter matrix  $\hat{Z}$ . This is a property which makes the LAVA method favour parsimonious models, meaning linear models with as few parameters as possible are favoured over nonlinear models with a large set of non-zero parameters.

## 2.4 Evaluation metrics

We use validation data that is separate from the identification data, as input to the identified model to simulate the controller output, which is then used to evaluate the model. The simulated controller output is computed recursively as

$$\hat{u}_s(t) = f\left(\hat{u}_s(t-1), \dots, \hat{u}_s(t-n_a), \hat{y}(t), \dots, \hat{y}(t-n_b+1); \hat{\Theta}, \hat{Z}\right), \quad (6)$$

where  $f(\cdot)$  is the function that corresponds to (5), and the simulation is performed for  $t = L, \dots, N$ , where  $L = \max(n_a, n_b) + 1$  and

$$\hat{u}_s(L-k) = \hat{u}(L-k), \quad k = 1, \dots, n_a. \quad (7)$$

We will use the RMSE and FIT metrics to evaluate the performance of the identified models. Here, we define the RMSE as the root of the average squared simulation errors

$$\text{RMSE} = \sqrt{\frac{1}{N} \sum_{t=1}^N \|\hat{u}_s(t) - u(t)\|_2^2}, \quad (8)$$

and the FIT metric as

$$\text{FIT} = 100 \left( 1 - \frac{\|u - \hat{u}_s\|_2}{\|u - \bar{u} \mathbf{1}\|_2} \right), \quad (9)$$

where  $\bar{u}$  is the empirical mean of  $u$  and  $\mathbf{1}$  is a vector of ones.

We also compare the number of elements in  $\hat{Z}$ ,  $n_z$ , to the number of identified nonzero elements, which is given by the  $l_0$ -norm,  $\|\hat{Z}\|_0$ . This will serve as a metric for sparsity.

### 3. SIMULATED STANDING HUMAN BALANCE

The state of a standing human is determined by the orientations and angular velocities of the body segments. For upright standing, the desired state is to have the legs and trunk aligned with the upright vertical orientation of the environment and that the angular velocities of these segments are zero. Deviations from this desired state are communicated to the CNS through the visual, vestibular and proprioceptive sensors. The CNS will then process this information and provide feedback by activating the appropriate muscles, which results in corrective joint torques. The feedback mechanism, which generates corrective joint torques in order to bring the state closer to the desired state, will be referred to as the neuromuscular controller.

A commonly used model of a standing human is the planar inverted double-pendulum model, where the lower pendulum segment represents the legs and the upper pendulum segment represents the upper body. The two joints in this model represent the ankle and hip joints. This model is motivated by the balancing strategies known as the ankle and hip strategies, which have been found to be the main contributing strategies in upright standing (Hof, 2007). Furthermore, a standing human is known to move predominantly in the sagittal plane, provided that the stance width is sufficient (Day et al., 1993).

The inverted double-pendulum has two degrees of freedom  $\phi_1$  and  $\phi_2$ , defined as the angles between the upright vertical direction and the leg and trunk segments, respectively. We will use subscript 1 to denote quantities attributed to the leg segment and ankle joint, and 2 for the upper body segment and hip joint. The output of the inverted double-pendulum system is  $y = [\phi_1 \ \phi_2 \ \dot{\phi}_1 \ \dot{\phi}_2]^\top$ , which contains the angular velocities in addition to the joint angles. The output of the neuromuscular controller are the joint torques  $T = [T_1 \ T_2]^\top$ . The external disturbance,  $d = [d_1 \ d_2]^\top$ , used to excite the system is added to  $T$ . Therefore, the input to the inverted double-pendulum is  $u = T + d$ . In addition to the external disturbance we add an internal disturbance  $v$ , which models biological noise that acts on the information that the neuromuscular controller receives from the biological sensors about the state of the system. A block-diagram of the standing human balance system is shown in Fig. 2.

The identification data obtained from inertial sensors consists of

$$\mathcal{D} = \left\{ \left( \hat{T}(t), \hat{y}(t) \right) \right\}, \quad t = 1, \dots, N, \quad (10)$$

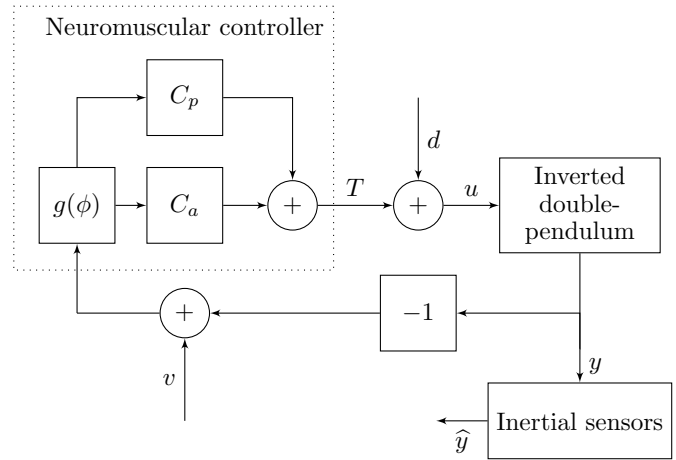


Fig. 2. A model of standing human balance as a closed loop system.

where  $\hat{y}$  is the estimated output of the inverted double-pendulum and  $\hat{T}$  is the estimated controller output.

*Simulation model.* The model of the neuromuscular controller that we use in our simulations is the same as used in Engelhart et al. (2016). This controller consists of a passive part  $C_p$  and an active part  $C_a$ . Both  $C_p$  and  $C_a$  contain a proportional and a derivative (PD) feedback from the joint angles, which means that the controller also uses angular velocity information  $\dot{\phi}_1$ ,  $\dot{\phi}_2$ . The  $C_a$  component models the part of the joint torque that comes from muscle activation via neural signals, and contains neural time delay and muscle activation dynamics. The reference signal is constant and corresponds to a zero vector, since a stable upright posture corresponds to  $\phi_1 = \phi_2 = 0$  and  $\dot{\phi}_1 = \dot{\phi}_2 = 0$ .

The equations of motion of the inverted double-pendulum model was calculated using Lagrangian formalism and then linearized using Taylor expansion to obtain a linear state-space model. Physical parameters of the inverted double-pendulum, such as mass, segment length and moment of inertia, were also taken from Engelhart et al. (2016).

The disturbance  $d$  was a two-dimensional multisine signal, where the periodic components had a 10 Nm amplitude. The periodic components were initialized at a random phase and excited 27 frequencies, which were logarithmically spaced in the frequency band between 0.05 Hz to 5 Hz. The disturbance signal was simulated for 80 s, which is equal to four periods of the lowest frequency component. After the first two periods, the sign of the  $d_2$  was inverted to make it independent of  $d_1$ , since both  $d_1$  and  $d_2$  excite the same frequencies. This is equivalent to the multiple experiment approach to excite MIMO systems when using multisine signals (Pintelon and Schoukens, 2012). The internal disturbance  $v$  was simulated as zero mean Gaussian noise with variance  $5 \times 10^{-3} \text{ rad}^2$  that is filtered through a first-order low pass filter with static gain 1 and time constant 1 s.

*Nonlinear controller.* A nonlinear controller in the form of a Hammerstein model, was also implemented by applying the following function to the input to the neuromus-

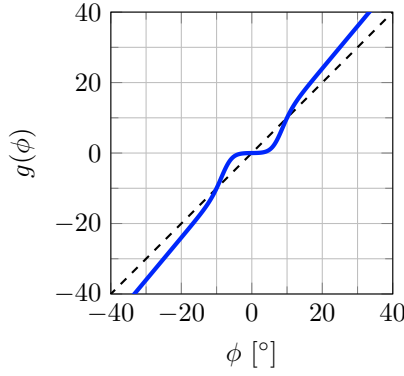


Fig. 3. The nonlinearity  $g(\phi)$  that was applied to the input of the neuromuscular controller (solid blue) compared to the line  $\phi$  (dashed black).

Table 1. Validation results for different models of the linear neuromuscular controller.

$n_a$	$n_b$	$n_z$	$\ \hat{Z}\ _0$	RMSE [Nm]	FIT [%]
0	1	0	0	(8.7 6.7)	(94.3 95.0)
0	2	0	0	(8.6 6.3)	(94.4 95.4)
0	3	0	0	(8.6 5.7)	(94.4 95.8)
0	4	0	0	(8.5 5.4)	(94.4 96.1)
0	5	0	0	(8.5 5.3)	(94.5 96.1)
0	6	0	0	(8.5 5.3)	(94.5 96.2)
0	6	162	65	(8.4 5.3)	(94.5 96.1)

Table 2. Validation results for different models of the nonlinear neuromuscular controller.

$n_a$	$n_b$	$n_z$	$\ \hat{Z}\ _0$	RMSE [Nm]	FIT [%]
0	1	0	0	(58.8 40.4)	(59.8 67.3)
0	2	0	0	(42.1 28.8)	(71.2 76.7)
0	3	0	0	(38.4 25.0)	(73.7 79.7)
0	4	0	0	(37.6 24.0)	(74.3 80.6)
0	5	0	0	(37.5 23.6)	(74.3 80.9)
0	6	0	0	(37.7 23.5)	(74.2 81.0)
0	6	162	76	(33.9 21.7)	(76.8 82.4)
0	6	1250	303	(28.5 19.5)	(80.5 84.2)

cular controller

$$g(\phi) = \frac{e^{\phi'-b}}{e^{\phi'-b} + 1} K\phi \quad (11)$$

$$\phi' = \frac{|\phi|\phi_0}{b - \ln(K-1)}, \quad (12)$$

which is a logistic sigmoid function that is modulated by the function  $K\phi$ . This nonlinearity has the effect that angles below  $\phi_0$  will be underestimated by the controller and angles above  $\phi_0$  will approach the line  $K\phi$  as  $|\phi| \rightarrow \infty$  for  $K \geq 0$ . Small angles will be close to zero and  $b \geq 0$  affects how flat the function is for small  $\phi$ . Fig.3 shows the nonlinearity  $g(\phi)$  for  $K = 1.2$ ,  $b = 5$  and  $\phi_0 = 10^\circ$ , which was used in the simulations to obtain data from a nonlinear neuromuscular controller. This static nonlinearity models the common hypothesis about human balance that small deviations from the equilibrium are not corrected by the neuromuscular controller.

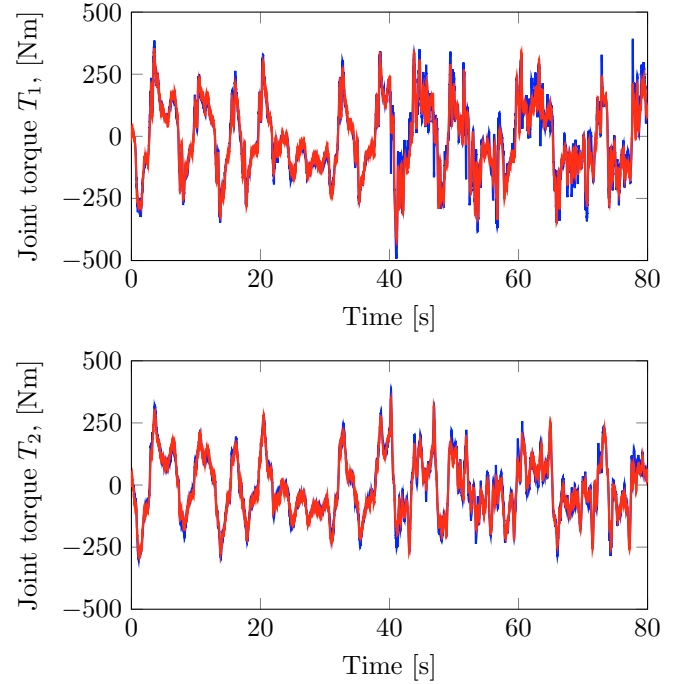


Fig. 4. The true simulated outputs  $T$  of the nonlinear neuromuscular controller (blue) and the simulated output from the identified model (red) for the validation data set.

*Measurement models.* Two inertial sensors were simulated to provide the data that was used to identify the neuromuscular controller. One sensor was attached to each segment of the inverted double-pendulum, and the sensors were oriented to have one axis parallel with the segment, and one axis parallel with the rotation axes of the joints. Zero mean Gaussian measurement noise was simulated with variance  $1 \times 10^{-2} \text{ m}^2/\text{s}^4$  for the accelerometer and  $1 \times 10^{-5} \text{ rad}^2/\text{s}^2$  for the gyroscope. These measurements were then used to obtain an estimate of the states  $\hat{y} = [\hat{\phi}_1 \ \hat{\phi}_2 \ \hat{\phi}'_1 \ \hat{\phi}'_2]^\top$ . The closed loop system of standing human balance was implemented in Simulink (MathWorks, Inc.). The system was sampled with a sample period of  $T_s = 0.01 \text{ s}$ .

We also need measurements of the joint torque  $T$ , generated by the neuromuscular controller, to be able to do identification. These are typically not available in a realistic situation, but can be estimated from the output of the system, so called *inverse dynamics*. A discrete-time state-space model of the inverted double-pendulum is used, which has the form

$$y(t+1) = Fy(t) + Gu(t). \quad (13)$$

Using the  $\hat{y}$  obtained from the inertial sensors, the joint torque can be estimated by solving the following optimization problem

$$\hat{u} = \arg \min_u \sum_{t=1}^{N-1} \|Gu(t) + F\hat{y}(t) - \hat{y}(t+1)\|_2^2 \quad (14)$$

$$+ \|\lambda(u(t+1) - u(t))\|_2^2$$

$$\hat{T} = \hat{u} - d, \quad (15)$$

where  $\lambda$  acts as a smoothing parameter to reduce the noise in the estimate. In our simulation  $\lambda = 0.0001$  was chosen. The optimization problem (14) was solved using a Gauss-Newton algorithm (Nocedal and Wright, 2006), with a sliding window containing 1000 samples and an overlap of 50 samples between consecutive windows.

### 3.1 Results and discussion

Four different data sets were simulated, two using the linear controller and two with the nonlinearity (11) applied to the controller input. Different data sets were used for estimation and validation and each data set contained  $N = 8000$  data points. Results for the identified models of the simulated neuromuscular controllers are summarized in Table 1 for the linear controller, and Table 2 for the nonlinear controller.

The simulated neuromuscular controller uses only joint angle and angular velocity information. Therefore,  $n_a = 0$  was used for all estimated models, so there is no dependence on past controller outputs. The parameter  $n_b$  controls up to how many past controller inputs that the linear model depend on, where  $n_b = 1$  means that the linear model only depend on current inputs. It can be seen that increasing  $n_b$  barely improves the accuracy for the model of the linear controller. Adding nonlinear parameters does not improve the accuracy, even though 65 nonzero nonlinear parameters were identified. The reason why some nonzero nonlinear parameters were found may be explained by the internal noise process  $v$ , which is a filtered white noise process, that is not observable by the inertial sensors. It would be interesting to investigate further, how the internal disturbance affects the identified model. Note also that the nonlinear parameters used in the identification in this example only depend on current controller inputs to keep the number of parameters low, whereas the linear predictor model depend on  $n_b - 1$  past controller inputs as well.

For the model of the nonlinear neuromuscular controller it is clear that a linear model is too restrictive, and that increasing  $n_b$  only improves the accuracy to some extent. Adding nonlinear parameters improved the accuracy further. As the the number of nonlinear parameters increased, less nonzero parameters were found relative to the total number of allowed nonlinear parameters. Fig. 4 shows the simulated output from the identified nonlinear model with best FIT when applied to the validation data.

## 4. POSITION SERVO

A position servo is a closed loop system that consists of a motor, an angular sensor and a feedback controller, where the motor axis angle  $\phi$  should follow a desired reference signal  $r$ . We define the control error as  $e = r - \phi$ , and the objective of the controller is to attain  $e = 0$ . To achieve this objective the controller will generate a control signal in the form of a voltage  $u$ , which is used to drive the motor. For this example we use a DC motor which operates in the voltage range of  $\pm 2.5V$ . The DC motor is connected to a flat circular disk, whose rotation angle  $\phi$  is to be controlled.

The identification data collected from each experiment was

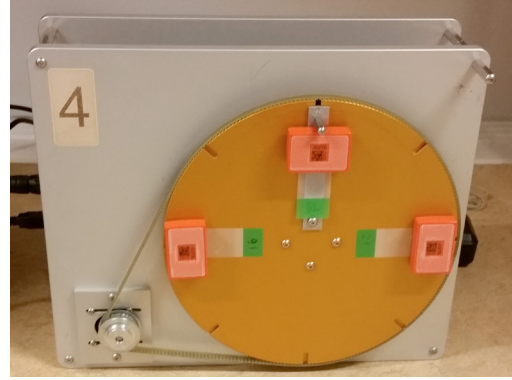


Fig. 5. The experimental setup for the position servo with inertial sensors attached.

$$\mathcal{D} = \left\{ \left( u(t), \hat{\phi}(t), \dot{\hat{\phi}}(t) \right) \right\}, \quad t = 1, \dots, N, \quad (16)$$

where the controller output  $u(t)$  is known exactly, since we have direct access to the implemented controller. The controller input consists of the estimated angle  $\hat{\phi}$  and angular velocity  $\dot{\hat{\phi}}$ . Thus, the inertial sensors provide more information than the controller uses. Note that the actual controller input are measurements of  $\phi$  that comes from an angular transducer built into the experimental setup, whereas the identification data comes from inertial sensors.

The controller used in the experiments is a lead-filter, with the transfer function

$$C(s) = \frac{0.4386s + 1.519}{0.8661s + 1}. \quad (17)$$

The controller was implemented on a computer, with a sample rate of  $T_s = 0.025s$ . The difference equation for this linear discrete-time controller has the form of

$$u(t) = 0.9715u(t-1) + 0.5064e(t) - 0.4632e(t-1). \quad (18)$$

A non-linear controller was also implemented, where a static non-linearity  $h$ , defined as

$$h(u, u_{min}, u_{max}) = \begin{cases} 0, & |u| < u_{min} \\ u, & u_{min} \leq |u| \leq u_{max} \\ u_{max}, & |u| > u_{max} \end{cases}, \quad (19)$$

which is a saturation and a dead zone, was applied to the controller output  $u(t)$  (18).

Three Xsens MTw wireless inertial sensors (Xsens, 2017), were attached to the circular disk and used to estimate the rotation angle and angular velocity of the disk. The experimental setup can be seen in Fig. 5. The disturbance signal  $d$  was an additional voltage signal, which was added to the controller output. Therefore, the actual input to the DC motor was  $u + d$ . The disturbance was generated as a multisine signal with 9 excited frequencies, logarithmically spaced in the frequency band between 0.2 Hz to 8 Hz. Each periodic component had a random initial phase and amplitude 0.3 V.

### 4.1 Results and discussion

Two data sets with  $N = 6802$  data points were collected using the linear controller (18) and with the added non-linearity (19) with  $u_{min} = 0.02V$  and  $u_{max} = 0.8V$ . The first half of each data set was used for estimation

Table 3. Validation results for different models of the linear servo controller.

$n_a$	$n_b$	$n_z$	$\ \widehat{Z}\ _0$	RMSE [V]	FIT [%]
0	1	0	0	0.1940	58.6
0	2	0	0	0.1740	62.8
1	1	0	0	0.0072	98.5
1	2	0	0	0.0067	98.6
1	2	243	0	0.0067	98.6

Table 4. Validation results for different models of the nonlinear servo controller.

$n_a$	$n_b$	$n_z$	$\ \widehat{Z}\ _0$	RMSE [V]	FIT [%]
0	1	0	0	0.2362	53.9
0	2	0	0	0.2338	54.4
1	1	0	0	0.3411	33.4
1	2	0	0	0.3342	34.8
0	2	81	18	0.1532	70.1
0	2	625	36	0.1523	70.3
1	2	243	31	0.0626	87.8
1	2	3125	89	0.0493	90.4

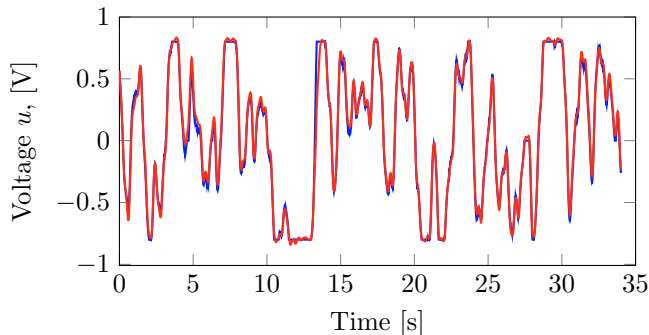


Fig. 6. The true output  $u$  of the nonlinear position servo controller (blue) and the simulated output from the identified model (red) for the validation data set.

and the second half for validation. The constant reference signal  $r = 0$  was used for all experiments. Results for the identified position servo controllers are summarized in Table 3 for the linear controller, and Table 4 for the nonlinear controller.

As the true controller depends on both current and past controller inputs as well as past controller outputs, we try different values for both  $n_a$  and  $n_b$ . The models of the linear controller were very accurate. Extending the model to include a nonlinear part resulted in only zero-valued nonlinear parameters, which shows that the method is able to identify a parsimonious model in this example.

For the models of the nonlinear controller it can be seen that linear models resulted in poor accuracy. Adding nonlinear parameters improved the model accuracy significantly. Even though as many as 3125 nonlinear parameters were allowed, only 89 were identified as nonzero, producing a simpler, sparse model. Fig. 6 shows the simulated output from the identified nonlinear model with best FIT when applied to the validation data.

## 5. CONCLUSION AND FUTURE WORK

In this paper we have investigated the properties of the LAVA method, when used to identify linear and nonlinear controllers operating in closed loop. Two examples were provided, a simulated standing human balance scenario and a real position servo using a DC motor. Identification data were obtained through external, inertial sensors. The LAVA method was able to identify sparse nonlinear models that described the dynamics of the nonlinear controllers. In the case of the linear position servo controller, a parsimonious linear model was identified, even though the model allowed for nonlinear parameters. In the case of the linear simulated balance controller some nonzero nonlinear parameters were identified, which did not improve the accuracy of the model.

A flexible model structure is desirable in the identification of real biological feedback systems, where linear models can be too restrictive. The studied method provides flexibility, yet favours the parsimonious, sparse models in identification. In a future study, we would like to apply the method to identify a real neuromuscular controller in human balance and compare the LAVA method with other nonlinear system identification methods.

## REFERENCES

- Day, B., Steiger, M., Thompson, P., and Marsden, C. (1993). Effect of vision and stance width on human body motion when standing: implications for afferent control of lateral sway. *The Journal of physiology*, 469(1), 479–499.
- Engelhart, D., Boonstra, T.A., Aarts, R.G.K.M., Schouten, A., and van der Kooij, H. (2016). Comparison of closed-loop system identification techniques to quantify multi-joint balance control. *Annual Reviews in Control*, 41, 58–70.
- Hof, A.L. (2007). The equations of motion for a standing human reveal three mechanisms for balance. *Journal of biomechanics*, 40(2), 451–457.
- Kok, M. (2016). *Probabilistic modeling for sensor fusion with inertial measurements*. Ph.D. thesis, Linköping University.
- Ljung, L. (1999). *System Identification: theory for the user*. Prentice Hall, Upper Saddle River, NJ, 2nd edition.
- Mattsson, P., Zachariah, D., and Stoica, P. (2018). Recursive nonlinear-system identification using latent variables. *Automatica*, 93, 343 – 351.
- Nocedal, J. and Wright, S. (2006). *Numerical Optimization*. Springer Series in Operations Research, 2nd edition.
- Pintelon, R. and Schoukens, J. (2012). *System Identification: A frequency domain approach*. John Wiley & Sons, Inc., Hoboken, NJ, 2nd edition.
- Solin, A. and Särkkä, S. (2014). Hilbert space methods for reduced-rank gaussian process regression. ArXiv preprint arXiv:1401.5508.
- Xsens (2017). MTw Awinda Wireless Motion Tracker. (Online) <https://www.xsens.com/download/pdf/documentation/mtw2-awinda/MTw2-Awinda.pdf> accessed December 2017.